ACS Catalysis

Research Article

pubs.acs.org/acscatalysis

Active Sites in Sn-Beta for Glucose Isomerization to Fructose and Epimerization to Mannose

Ricardo Bermejo-Deval,[‡] Marat Orazov,[‡] Rajamani Gounder,[†] Son-Jong Hwang, and Mark E. Davis*

Chemical Engineering, California Institute of Technology, Pasadena, California 91125, United States

Supporting Information

ABSTRACT: Framework Lewis acidic tin sites in hydrophobic, pure-silica molecular sieves with the zeolite beta topology (Sn-Beta) have been reported previously to predominantly catalyze glucose–fructose isomerization via 1,2 intramolecular hydride shift in water and glucose–mannose epimerization via 1,2 intramolecular carbon shift in methanol. Here, we show that alkali-free Sn-Beta predominantly isomerizes glucose to fructose via 1,2 intramolecular hydride shift in both water and methanol. Increasing extents of postsynthetic Na^+ exchange onto Sn-Beta, however, progressively shifts the reaction pathway toward glucose–mannose epimerization via 1,2 intramolecular carbon shift. Na^+ remains exchanged onto silanol groups proximal to Sn centers during reaction in methanol solvent, leading to nearly exclusive selectivity toward epimerization. In contrast, decationation occurs with increasing reaction time in aqueous solvent and gradually shifts the reaction selectivity to isomerization at the expense of epimerization. Decationation and the concomitant selectivity changes are mitigated by the addition of NaCl to the aqueous reaction solution. Preadsorption of ammonia onto Sn-Beta leads to near complete suppression of infrared and ^{119}Sn nuclear magnetic resonance spectroscopic signatures attributed to open Sn sites and of glucose–fructose isomerization pathways in water and methanol. These data provide evidence that Lewis acidic open Sn sites with either proximal silanol groups or Na-exchanged silanol groups are respectively the active sites for glucose–fructose isomerization and glucose–mannose epimerization.

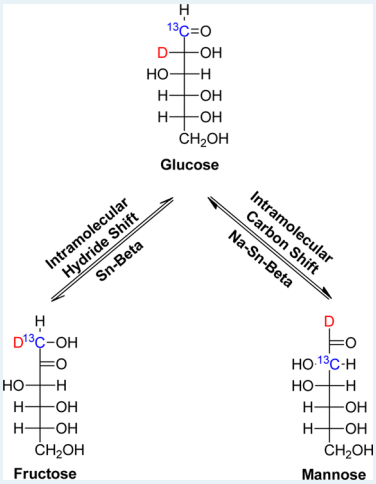

KEYWORDS: *tin-beta, open site, closed site, silanol, Bilik reaction, epimerization, isomerization, fructose, glucose, mannose, sodium exchange*

1. INTRODUCTION

We have previously shown that tetravalent Lewis acidic metal centers (Sn^{4+} and Ti^{4+}) isolated within hydrophobic, pure-silica molecular sieves with the zeolite beta framework topology (Sn-Beta and Ti-Beta, respectively) catalyze the isomerization of glucose to fructose in aqueous media.[1−4] Framework Sn sites mediate the ring-opening of glucose and coordinate with glucose O1 and O2 atoms prior to isomerization via an intramolecular hydride shift from the C2 to C1 position (1,2 intramolecular hydride shift) in the ring-opened glucose chain.[1] This glucose isomerization reaction pathway is analogous to that observed in metalloenzymes such as D-xylose isomerase XI that contain two divalent Lewis acid metal centers (e.g., Mg^{2+} or Mn^{2+}) confined within a hydrophobic pocket.[5−7] Extra-framework SnO_x clusters located within hydrophobic micropores of pure-silica zeolite beta, but not at external crystallite surfaces or on amorphous supports, are also able to isomerize glucose to fructose in aqueous solutions. Unlike the framework Sn centers, however, these extra-framework intrazeolitic SnO_x clusters act as solid bases that catalyze glucose isomerization via LdB–AvE (Lobry de Bruyn–Alberda van Ekenstein) rearrangements involving enolate intermediates,[2,8] and the hydrophobic surrounding voids appear to protect SnO_x surface sites from inhibition or deactivation that otherwise occurs in the presence of liquid water.

When Sn-Beta was used to react glucose in methanol solvent, we obtained the surprising result that mannose was produced selectively via a Lewis acid-mediated 1,2 intramolecular carbon shift mechanism known as the Bilik reaction.[2] Although homogeneous molybdate anions[9−11] and nickel(II) diamine complexes[12−14] have been reported to catalyze the epimerization of glucose to mannose by the Bilik reaction, Sn-Beta is the first example of a heterogeneous catalyst that can mediate this reaction.[2] Only framework Sn sites in Sn-Beta were able to form mannose via the Bilik reaction in methanol, as intrazeolitic SnO_x clusters isomerized glucose to fructose by base-catalyzed LdB–AvE rearrangement as also occurred in water.[2] SnO_x clusters deposited on external zeolite crystal surfaces and on amorphous silica also isomerized glucose to fructose in liquid methanol by the enolate mechanism,[2] in contrast with their inability to do so in liquid water. Thus, only zeolites that contained framework Sn sites showed differences in the

Received: April 8, 2014
Revised: May 29, 2014
Published: June 2, 2014

   dx.doi.org/10.1021/cs500466j | ACS Catal. 2014, 4, 2288−2297

predominant mechanism by which glucose is reacted in aqueous and methanol solvent.

Framework Sn centers in Sn-Beta were proposed by Corma et al.[15] to be present in both "closed" and "open" forms that respectively correspond to a nonhydrolyzed Sn site ($Sn\text{-}(OSi)_4$) and a partially hydrolyzed Sn site ($(HO)\text{-}Sn\text{-}(OSi)_3$) (Scheme 1a and b, respectively). The open site was proposed to be more

Scheme 1. Schematic Representation of the Dehydrated States of (a) Closed and (b) Open Sites in Sn-Beta, (c) the Na-Exchanged Open Site, and (d) the NH_3-Dosed Open Site[a]

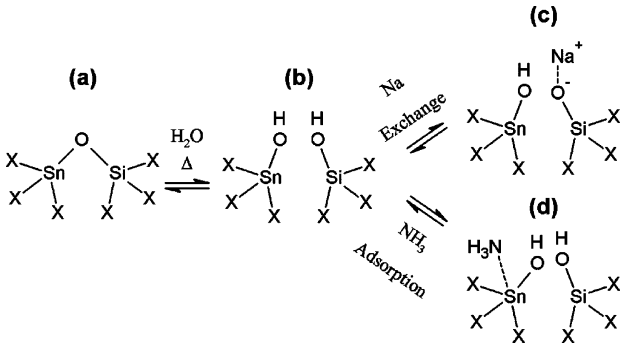

[a]"X" denotes framework O−Si units.

reactive in the Baeyer−Villiger oxidation of cyclic ketones,[15] and we have also similarly proposed the open site to be more reactive in the isomerization of glucose to fructose.[1] Previously, we attempted to increase the proportion of open Sn sites by substitution of $SnCl_4$ precursors with $Sn(CH_3)Cl_3$ during crystallization and subsequent Na^+ exchange prior to calcination to prevent condensation of proximal Sn−OH and Si−OH groups.[1] The reactivity of these modified Sn-Beta samples were indistinguishable from Sn-Beta crystallized using $SnCl_4$ precursors, indicating that open and closed Sn sites were interconvertible during calcination and reaction conditions.[1] As a result, while we were able to distinguish between open and closed Sn sites in Sn-Beta in ^{119}Sn NMR spectra, our previous experimental data could not conclusively determine which site (or both) was the active site for glucose isomerization.[1]

Quantum chemical studies suggest that glucose−fructose isomerization pathways are catalyzed with lower barriers on open than on closed sites.[1] Khouw and Davis[16] exchanged Na^+ onto silanol groups adjacent to open Ti sites ($(HO)\text{−}Ti\text{−}(OSi)_3$) in TS-1 and completely inhibited catalytic alkane oxidation reactions with hydrogen peroxide,[16] providing conclusive evidence that open Ti sites were the active sites for alkane oxidation. Thus, it seems plausible that the silanol group adjacent to the open Sn site in Sn-Beta could influence the rates and selectivities of glucose isomerization catalysis. Rai et al.[17] used density functional theory to calculate a lower energy glucose−fructose isomerization pathway when glucose binds to an open Sn site in a monodentate mode that involves the adjacent silanol group, relative to that when glucose binds to an open Sn site in a bidentate mode that does not involve the neighboring silanol group. Conversely, the bidentate binding mode results in a lower energy pathway for glucose−mannose epimerization than does the monodentate binding mode.[17] If epimerization is a lower energy pathway than isomerization when silanol groups adjacent to Sn sites are not involved in the mechanism, a detail that is not addressed by Rai et al.,[17] then our previous experimental results[2] suggest that active sites in Sn-Beta in methanol may be altered in a manner that precludes the involvement of the neighboring silanol in the reaction pathway.

Here, we provide new experimental results that further examine the structure of active Sn sites in Sn-Beta and their influence on glucose isomerization and epimerization reactivity. The mechanistic role of the silanol group adjacent to the open Sn site is examined by exchanging its proton with a sodium cation. We provide evidence that Na-exchanged Sn-Beta catalyzes the epimerization of glucose to mannose via 1,2 intramolecular carbon shift with high selectivity in methanol and in concentrated aqueous NaCl solutions. In water, the selectivity to isomerization to fructose via 1,2 intramolecular hydride shift increases with reaction time because Na^+ ions are removed during reaction and neighboring silanol groups are restored. These data clearly show that the open Sn site is the active site for both glucose isomerization and epimerization reactions, with isomerization prevailing when adjacent silanol groups are in their proton form and epimerization prevailing when adjacent silanol groups are exchanged with Na^+.

2. EXPERIMENTAL METHODS

2.1. Synthesis of Sn-Beta, ^{119}Sn-Beta, Na-Sn-Beta, and Si-Beta. Sn-Beta and ^{119}Sn-Beta were synthesized according to previously reported procedures.[1] A total of 15.25 g of tetraethylammonium hydroxide solution (Sigma-Aldrich, 35% (w/w) in water) was added to 14.02 g of tetraethylorthosilicate (Sigma-Aldrich, 98% (w/w)), followed by the addition of 0.172 g of tin(IV) chloride pentahydrate (Sigma-Aldrich, 98% (w/w)) or of 0.121 g of ^{119}Sn enriched tin(IV) chloride pentahydrate (Cambridge Isotopes, 82% isotopic enrichment). The mixture was stirred until tetraethylorthosilicate was completely hydrolyzed and then allowed to reach the targeted H_2O/SiO_2 ratio by complete evaporation of ethanol and partial evaporation of water. Finally, 1.53 g of HF solution (Sigma-Aldrich, 54% (w/w) in water) was added, resulting in the formation of a thick gel. The final molar composition of the gel was 1 SiO_2/0.0077 $SnCl_4$/0.55 TEAOH/0.54 HF/7.52 H_2O. As-synthesized Si-Beta (vide infra) was added as seed material (5 wt % of SiO_2 in gel) to this gel and mixed. The final gel was transferred to a Teflon-lined stainless steel autoclave and heated at 413 K in a static oven for 40 days. The recovered solids were centrifuged, washed extensively with water, and dried at 373 K overnight. The dried solids were calcined in flowing air (1.67 $cm^3\ s^{-1}$, Air Liquide, breathing grade) at 853 K (0.0167 K s^{-1}) for 10 h to remove the organic content located in the crystalline material. ^{119}Sn-Beta was calcined twice under the same conditions.

Na-Sn-Beta was synthesized using the same procedure as Sn-Beta, but with the addition of $NaNO_3$ (Sigma-Aldrich, ≥99.0%) to the synthesis gel. The final molar composition of the gel was 1 SiO_2/x $NaNO_3$/0.0077 $SnCl_4$/0.55 TEAOH/0.54 HF/7.52 H_2O, where "x" was 0.010, 0.017, and 0.033 (Na-Sn-Beta-100, -60, and -30, respectively). The gel was transferred to a Teflon-lined stainless steel autoclave and heated at 413 K in a static oven for 25 days. The recovered solids were washed, dried, and calcined using the same procedure as for Sn-Beta. Synthesis gels with a Si/Na ratio lower than 30 yielded a heterogeneous material with small black particles dispersed among the zeolite. These black particles were separated from the zeolite by hand and were found to be amorphous, having a Si/Sn and Na/Sn ratio of 15 and 2.28, respectively.

dx.doi.org/10.1021/cs500466j | ACS Catal. 2014, 4, 2288−2297

Si-Beta was prepared by adding 10.01 g of tetraethylammonium fluoride dihydrate (Sigma-Aldrich, 97% (w/w) purity) to 10 g of water and 4.947 g of tetraethylorthosilicate (Sigma-Aldrich, 98% (w/w)). This mixture was stirred overnight at room temperature in a closed vessel to ensure complete hydrolysis of the tetraethylorthosilicate. The targeted H_2O/SiO_2 ratio was reached by complete evaporation of the ethanol and partial evaporation of the water. The final molar composition of the gel was SiO_2/0.55 TEAF/7.25 H_2O. The gel was transferred to a Teflon-lined stainless steel autoclave and heated at 413 K in a rotation oven (60 rpm) for 7 days. The solids were recovered by filtration, washed extensively with water, and dried at 373 K overnight. The dried solids were calcined in flowing air (1.67 $cm^3\ s^{-1}$, Air Liquide, breathing grade) at 853 K (0.0167 K s^{-1}) for 10 h to remove the organic content located in the crystalline material.

2.2. Na^+ and H^+ Ion Exchange of Zeolite Samples. Each ion exchange step was carried out for 24 h at ambient temperature, using 45 mL of exchange or wash solution per 300 mg of starting solids. For the procedures involving multiple ion-exchange steps, the ion-exchange solution was replaced every 24 h without intermediate water washing. One, two, and three successive sodium ion exchanges (Sn-Beta-1Ex, Sn-Beta-2Ex, and Sn-Beta-3Ex, respectively) were performed by stirring calcined Sn-Beta in a solution of 1 M $NaNO_3$ (Sigma-Aldrich, ≥99.0%) and 10^{-4} M NaOH (Alfa Aesar 97%) in distilled water. The final material was recovered by centrifugation, and washed three times with 1 M $NaNO_3$ in distilled water. Acid-washed Sn-Beta (Sn-Beta-AW) was made by stirring the triply sodium-exchanged Sn-Beta (Sn-Beta-3Ex) in 1 M H_2SO_4 (Macron Fine Chemicals, >51%) for 1 h at ambient temperature, followed by separation by filtration and washing with 1 L of distilled water in 100 mL batches. Finally, the material was dried in room temperature air and calcined in flowing air (1.67 $cm^3\ s^{-1}$, Air Liquide, breathing grade) at 853 K (0.0167 K s^{-1}). We note that the dehydration of sodium-exchanged materials resulted in changes in their catalytic properties; therefore, to ensure comparable saturation of the samples with water, 24 h prior to reaction testing, all samples were placed in a chamber whose humidity was controlled by a saturated NaCl solution.

2.3. Ammonia Adsorption onto Sn-Beta. Ammonia gas dosing experiments were performed on Sn-Beta samples after drying in a Schlenk flask at 473 K for 2 h under a vacuum. The dried Sn-Beta was cooled under a dynamic vacuum to ambient temperature, and the flask was backfilled with 101 kPa of anhydrous ammonia gas (Matheson Tri-Gas, 99.99%). After 24 h, the excess ammonia was evacuated, and the sample was exposed to the atmosphere (Sn-Beta-NH_3). The ammonia-saturated material was regenerated by calcination (Sn-Beta-NH_3-Cal) in flowing air (1.67 $cm^3\ s^{-1}$, Air Liquide, breathing grade) for 6 h at 853 K (0.0167 K s^{-1}).

2.4. Characterization Methods. Scanning electron microscopy (SEM) with Energy Dispersive X-ray Spectroscopy (EDS) measurements were recorded on a LEO 1550 VP FE SEM at an electron high tension (EHT) of 15 kV. The crystalline structures of zeolite samples were determined from powder X-ray diffraction (XRD) patterns collected using a Rigaku Miniflex II diffractometer and Cu Kα radiation.

Ar adsorption isotherms at 87 K were obtained using a Quantachrome Autosorb iQ automated gas sorption analyzer. Zeolite samples were degassed at 353 K (0.167 K s^{-1}) for 1 h, 393 K (0.167 K s^{-1}) for 3 h, and 623 K (0.167 K s^{-1}) for 8 h prior to recording dry sample weight. For Sn-Beta-NH_3, the temperature during the degassing procedure never exceeded 473 K (0.167 K s^{-1}). Relative pressures (P/P_0) were measured between 10^{-7} and 1 at 87 K with precise volumetric Ar doses.

Deuterated acetonitrile dosing and desorption experiments were performed according to the procedure described elsewhere.[18] A Nicolet Nexus 470 Fourier transform infrared (FTIR) spectrometer with a Hg−Cd−Te (MCT) detector was used to record spectra in 4000−650 cm^{-1} range with a 2 cm^{-1} resolution. Self-supporting wafers (10−20 mg cm^{-2}) were pressed and sealed in a heatable quartz vacuum cell with removable KBr windows. The cell was purged with air (1 $cm^3\ s^{-1}$, Air Liquide, breathing grade) while heating to 373 K (0.0167 K s^{-1}), where it was held for 12 h, followed by evacuation at 373 K for >2 h (<0.01 Pa dynamic vacuum; oil diffusion pump), and cooling to 308 K under a dynamic vacuum. CD_3CN (Sigma-Aldrich, 99.8% D atoms) was purified by three freeze (77 K), pump, thaw cycles, then dosed to the sample at 308 K until the Lewis acid sites were saturated. At this point, the first FTIR spectrum in the desorption series was recorded. The cell was evacuated down to 13.3 Pa, and the second spectrum was recorded. Then, the cell was evacuated under a dynamic vacuum while heating to 433 K (0.0167 K s^{-1}). Concurrently, a series of FTIR spectra were recorded (2 min for each spectrum) at 5 min intervals. The resulting spectra were baseline-corrected, and the most illustrative spectra were chosen for presentation. The spectra are not normalized by the number of Sn sites. Spectral artifacts known as "interference fringes" were removed using a computational method based on digital filtering techniques and Fourier analysis.[19]

Solid-state magic angle spinning nuclear magnetic resonance (MAS NMR) measurements were performed using a Bruker Avance 500 MHz spectrometer equipped with a 11.7 T magnet and a Bruker 4 mm broad band dual channel MAS probe. The operating frequencies were 500.2 and 186.5 MHz for ^1H and ^{119}Sn nuclei, respectively. Approximately 60−80 mg of powder was packed into 4 mm ZrO_2 rotors and spun at 14 kHz for MAS or cross-polarization (CP) MAS experiments under ambient conditions. The $^{119}Sn\{^1H\}$ CP condition was optimized at a radiofrequency pulse power of 62.5 kHz ± ν_r, where ν_r is spinning frequency, and spectra were recorded using a 2 ms contact time. The recycle delay times were 20 and 2 s for ^{119}Sn MAS and CPMAS experiments, respectively. Signal averaging over 8000 scans was performed for the CPMAS spectrum of ^{119}Sn-Beta dehydrated after NH_3 dosing, while averaging over 30 000 scans was performed for the CPMAS spectrum of ^{119}Sn-Beta dehydrated after three Na-exchanges.

Liquid ^{13}C NMR spectra were recorded using a Varian INOVA 500 MHz spectrometer equipped with an auto-x pfg broad band probe. Carbon chemical shifts are reported relative to the residual solvent signal. ^{13}C NMR spectra were acquired with 2000 scans.

2.5. Reaction Procedures. Reactions with D-glucose (Sigma-Aldrich, ≥99%) were conducted in 10 mL thick-walled glass reactors (VWR) that were heated in a temperature-controlled oil bath. Reactions were prepared with a 1:100 Sn/glucose molar ratio using 5.0 g of a 1% (w/w) glucose solution with approximately 20 mg of catalyst. For reactions performed to investigate the effects of addition of NaCl to aqueous glucose reactant solution, 0.2 g of NaCl were added per 1.0 g of 1% (w/w) glucose solution. Reactors were placed in the oil bath at 353 K, and approximately 50 mg aliquots were extracted at 10, 20, and 30 min. These reaction aliquots were mixed with 50 mg of

dx.doi.org/10.1021/cs500466j | ACS Catal. 2014, 4, 2288−2297

a 1% (w/w) D-mannitol (Sigma-Aldrich, ≥98%) solution as an internal standard for quantification, diluted with 0.3 mL of H_2O, and filtered with a 0.2 μm PTFE syringe filter.

Glucose conversions and product yields were calculated by

$$X_{Gluc}(t) = \frac{n_{Gluc}(t=0) - n_{Gluc}(t)}{n_{Gluc}(t=0)} \times 100\ [\%] \quad (1)$$

$$Y_i(t) = \frac{n_i(t)}{n_{Gluc}(t=0)} \times 100\ [\%] \quad (2)$$

where $X_{Gluc}(t)$ is the glucose conversion at time t, in percent; $Y_i(t)$ is the fructose or mannose yield at time t, in percent; $n_{Gluc}(t=0)$ is the initial moles of glucose in the reactor; $n_{Gluc}(t)$ is the moles of glucose in the reactor at time t; and $n_i(t)$ is the moles of fructose or mannose in the reactor at time t.

Recyclability experiments were performed with Sn-Beta-3Ex reacted with glucose in water and methanol under the previously stated reaction conditions (353 K for 30 min in a 1% (w/w) with 1:100 Sn/glucose molar ratio) and washed once with the solvent used in the reaction. The solids were centrifuged and dried with ambient temperature air.

Reaction aliquots were analyzed by high performance liquid chromatography (HPLC) using an Agilent 1200 system (Agilent) equipped with diode array and evaporative light scattering detectors. Glucose, fructose, mannose, and mannitol fractions were separated with a Hi-Plex Ca column (6.5 × 300 mm, 8 μm particle size, Agilent) held at 358 K, using ultrapure water as the mobile phase at a flow rate of 0.6 mL s^{-1}.

Reactions with labeled ^{13}C glucose at the C1 position (Cambridge Isotope Laboratories, 1-^{13}C D-glucose, 98−99%) and deuterium (D) in the C2 position of glucose (Cambridge Isotope Laboratories, D-glucose-D2, >98%) were conducted under the same conditions as those with D-glucose. The reaction was ended by quenching after 30 min. The reaction solution was filtered and rotavaporated to separate the solvent from the reactant−product mixture. These recovered solids were dissolved in deuterium oxide and analyzed using ^{13}C NMR.

3. RESULTS AND DISCUSSION

3.1. Characterization of Microporous Materials. The powder X-ray patterns of Sn-Beta, Sn-Beta-1Ex, Sn-Beta-2Ex, Sn-Beta-3Ex, Sn-Beta-AW, Sn-Beta-NH_3, Sn-Beta-NH_3-Cal and Na-Sn-Beta (Si/Na = 100, 60 and 30) (Supporting Information Figures S.1 and S.2) show that each of the samples is highly crystalline and has the zeolite beta framework topology. No diffraction lines were observed at 2θ values of 26.7° and 34.0° that are characteristic of bulk SnO_2. SEM images (Supporting Information Figure S.3) indicate that the crystallite size of Sn-Beta is between 5 and 8 μm, and does not change significantly after exchange with $NaNO_3$/NaOH or treatment with NH_3. Na-Sn-Beta-30 (SEM images in Supporting Information Figure S.4) and other materials with gel Si/Na ratios >30 (results not presented here because of the high impurity content) contain an impurity that consists of dark, amorphous (by powder XRD) particles that are not observed in Na-Sn-Beta-60 and Na-Sn-Beta-100. Thus, synthesis gels with high amounts of Na formed contaminating amorphous solids with high Na and Sn contents (Si/Sn = 15, Na/Sn = 2.28). Bellusi et al.[20] proposed that the insertion of titanium into the silicate framework (TS-1) is inhibited when alkali metal ions are present in the synthesis gel due to the formation of alkali titanates. Here, it is possible that the Sn atoms in the synthesis gels form alkali stannates that are part of the amorphous phase impurity, thereby lowering the Sn and Na content of the crystalline Na-Sn-Beta that is formed.

The total micropore volumes of the samples were determined from Ar adsorption isotherms (87 K, Supporting Information Figures S.5−S.14) and are listed in Table 1. The micropore volumes of all Na exchanged materials decreased, perhaps because of excess $NaNO_3$ that remains on the solid after Na exchange. The final wash in the exchange procedure was performed with 1 M $NaNO_3$ because washing with distilled water results in partial Na^+ removal. The FTIR spectra (Figure S.15) of the Na exchanged materials indeed show a broad shoulder in the 1300 to 1500 cm^{-1} range as would be expected for the NO_3^- ion.[21] Sn-Beta-AW has the same micropore volume (0.19 $cm^3\ g^{-1}$) as the parent Sn-Beta material, showing that the measured decrease in microporosity for the Na-exchanged materials is not due to a loss of crystallinity, but likely due to the excess $NaNO_3$. Na-Sn-Beta-60 and Na-Sn-Beta-100 exhibit a similar micropore volume to Sn-Beta (Table 1), but Na-Sn-Beta-30 has a lower micropore volume of 0.14 $cm^3\ g^{-1}$. This significant decrease in micropore volume is likely due to the amorphous particle impurities. The ammonia-dosed Sn-Beta showed a lower micropore volume of 0.17 $cm^3\ g^{-1}$, which increased to that of the parent Sn-Beta sample after calcination (0.19 $cm^3\ g^{-1}$).

Table 1. Site and Structural Characterization of Samples Used in This Study

catalyst	Si/Sn[a]	Na/Sn[a]	Ar micropore volume[b] ($cm^3\ g^{-1}$)	IR bands[c] (cm^{-1})
Sn-Beta	95	0.00	0.19	2315, 2307, 2276, and 2266
Sn-Beta-1Ex	115	3.80	0.16	2310, 2280, and 2274
Sn-Beta-2Ex	159	4.38	0.15	2310, 2280, and 2274
Sn-Beta-3Ex	140	4.85	0.16	2310, 2280, and 2274
Sn-Beta-AW	104	0.27	0.19	2315, 2307, 2276, and 2266
Na-Sn-Beta-100	113	0.12	0.18	n.d.[d]
Na-Sn-Beta-60	127	0.26	0.19	n.d.[d]
Na-Sn-Beta-30	91	0.94	0.15	2310, 2280, and 2274
Sn-Beta-NH_3	105	0.00	0.17	2306 and 2270
Sn-Beta-NH_3-Cal	117	0.00	0.19	2315, 2307, 2276, and 2266

[a]Determined by Energy Dispersive X-ray Spectroscopy (EDS). The highest measured Si/Sn standard deviation for three scans of different parts of the same material was ±30, while the highest Na/Sn standard deviation was of ±1.25. These maximal standard deviations may be used to estimate the uncertainty of measurement for all samples. [b]Determined from the Ar adsorption isotherm (87 K). [c]After CD_3CN adsorption. [d]n.d., not determined.

Table 1 lists the Sn and Na contents for all of the samples in this study. The Na/Sn ratio increased with the number of consecutive sodium ion exchanges, with the highest ratio being 4.38 after three consecutive exchanges with $NaNO_3$/NaOH. Na/Sn ratios above unity likely reflect the presence of excess $NaNO_3$ deposited on the sample and some Na exchange occurring at silanol groups other than the ones adjacent to

dx.doi.org/10.1021/cs500466j | ACS Catal. 2014, 4, 2288−2297

open Sn centers. Acid treatment removed most of the sodium from the zeolite, as the Na/Sn ratio in Sn-Beta-AW decreased to 0.27. The Na/Sn ratio in the solids synthesized in the presence of sodium (Na-Sn-Beta-100, -60, and -30) as the sodium concentration increased in the synthesis gels.

3.2. Structural Characterization of the Sn Sites in Sn-Beta. The nature of Lewis acidic Sn sites in Sn-Beta and postsynthetically treated Sn-Beta samples was probed by monitoring changes in IR bands for C≡N stretching vibrations of adsorbed deuterated acetonitrile (2260−2340 cm^{-1})[22] during temperature-programmed desorption experiments (Figures 1 and S.16−S.19). The IR spectra for Sn-Beta exposed to

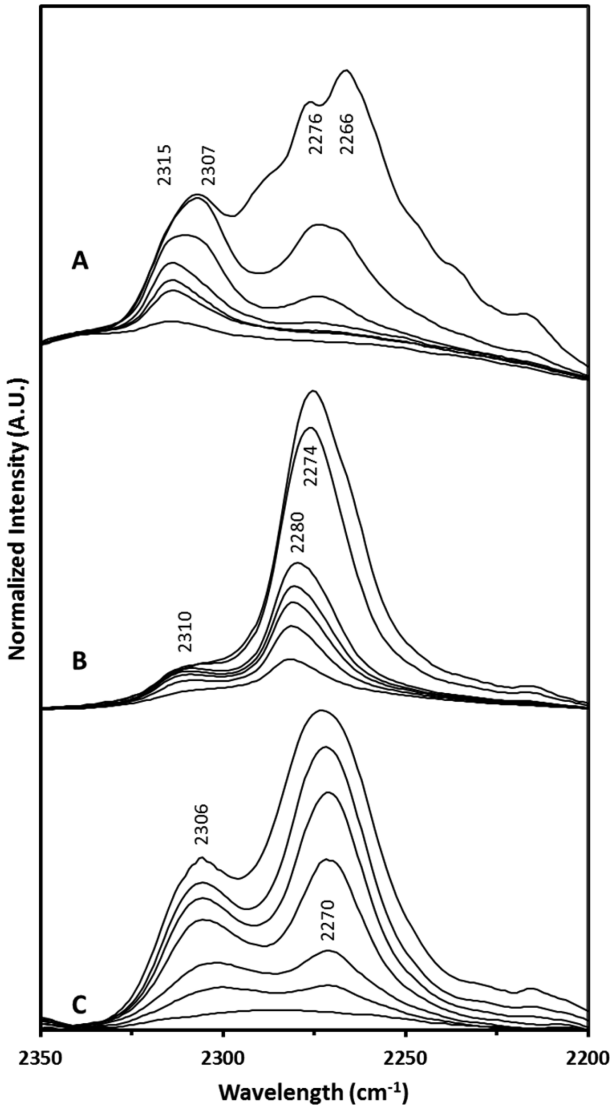

Figure 1. Baseline corrected IR spectra with decreasing CD_3CN coverage on (a) Sn-Beta, (b) Sn-Beta-3Ex, and (c) Sn-Beta-NH_3.

CD_3CN show bands at 2315, 2307, 2276, and 2266 cm^{-1} (Figure 1a). The CD_3CN IR bands at 2276 and 2266 cm^{-1} have been assigned to CD_3CN coordinated to silanol groups and physisorbed CD_3CN, respectively, while the bands at 2315 and 2307 cm^{-1} have been assigned to CD_3CN coordinated to Lewis acid sites.[22,23] These results are consistent with Corma et al.,[15] who assigned the 2316 cm^{-1} band to CD_3CN bound at the open Sn site and the 2308 cm^{-1} band to CD_3CN bound at a weaker Lewis acid site proposed to be the closed Sn site.

After $NaNO_3$/NaOH treatments (Figures 1b, S.16, and S.17), IR bands associated with CD_3CN bound to the open and closed sites disappear or diminish in intensity, while a single broad IR band with low intensity appears at ∼2310−2312 cm^{-1}. We speculate that this broad band may reflect multiple contributions from residual nonexchanged Sn sites, by extension of previous reports by Corma et al.[24] showing that a similar broad band at 2310 cm^{-1} in Sn-MCM-41 may be deconvoluted into multiple bands that correspond to different Sn environments. Interestingly, a more prominent IR band appears at 2280 cm^{-1} in Na-exchanged Sn-Beta materials (Figures 1b, S.16, and S.17), which we tentatively associate with the Lewis acid site responsible for the reactivity of these samples. The lower frequency of this new band (2280 cm^{-1}) compared to the open Sn site in Sn-Beta (2315 cm^{-1}) may suggest a weaker interaction[22] of CD_3CN with Lewis acid sites in Na-exchanged Sn-Beta. The CD_3CN that gives rise to the 2280 cm^{-1} band, however, desorbs more slowly than CD_3CN bound to the closed site (2307 cm^{-1}) and at comparable rates to CD_3CN bound to the open site (Figure 1a and b). These findings suggest that, in addition to the direct electron donation of CD_3CN to the Lewis acidic Sn center, secondary interactions of CD_3CN with the site or its surrounding environment may influence the binding strength and thus the ν(C≡N) of CD_3CN. Strongly bound CD_3CN at 2280 cm^{-1} (Figure S.18) was not present on Na-exchanged Si-Beta, confirming that this IR band is not a result of CD_3CN adsorbed to Na-exchanged terminal silanol groups and requires the presence of a framework Sn site. The synthetic Na-Sn-Beta-30 sample showed a similar desorption profile to that of Na-exchanged Sn-Beta (Figure S.19), suggesting that Na^+ ions introduced during or after synthesis have similar effects on the ability of Lewis acid sites in Sn-Beta to bind CD_3CN.

CD_3CN adsorption onto Sn-Beta-NH_3 gives rise to IR bands at 2306 cm^{-1}, associated with the closed Sn sites (as confirmed by ^{119}Sn NMR, vide infra) and a previously unobserved band at 2270 cm^{-1} (Figure 1c) for sites that desorb CD_3CN at a rate similar to that of the closed sites. The IR band of CD_3CN bound to the open site at 2315 cm^{-1} was not observed (Figure 1c). These data indicate that NH_3 remains bound only to open Sn sites in Sn-Beta-NH_3 after exposure to ambient air and treatment in a vacuum at 373 K prior to CD_3CN exposure (Scheme 2), consistent with proposals that open Sn sites are stronger Lewis acid sites than closed sites.[15] We propose that

Scheme 2. Schematic Representation of Open (top row) and Closed (bottom row) Sites in Sn-Beta after Different Treatment Procedures[a]

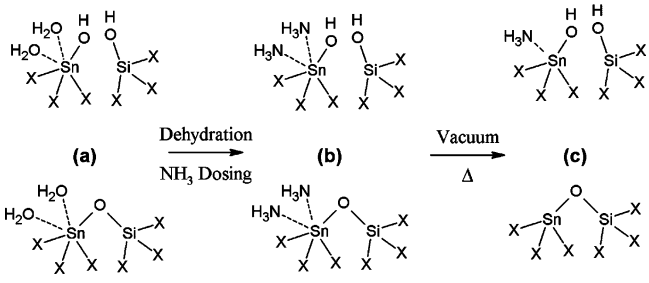

[a](a) Hydrated open and closed sites after (b) dehydration and saturation with NH_3, followed by subsequent (c) exposure to ambient atmosphere and heated evacuation (373 or 393 K for IR and NMR studies, respectively). "X" denotes framework O−Si units.

dx.doi.org/10.1021/cs500466j | ACS Catal. 2014, 4, 2288−2297

open Sn sites with bound NH_3 in Sn-Beta-NH_3 (Scheme 1d) are more electron-rich, and in turn bind CD_3CN more weakly, than open Sn sites without NH_3 ligands in Sn-Beta (Scheme 1b). The open Sn site with preadsorbed NH_3 (Scheme 1d) seems to be a likely candidate for the IR band at 2270 cm^{-1} (Figure 1c), which arises from weakly bound CD_3CN that disappears more rapidly than the IR band at 2315 cm^{-1} for CD_3CN bound at open Sn sites (Figure 1a). The presence of the 2306 cm^{-1} IR band in Sn-Beta-NH_3 suggests that any NH_3 initially bound to the closed site (Scheme 2b) desorbs after exposure to ambient air or vacuum treatment at 373 K (Scheme 2c) and forms a closed Sn site similar to that found in the untreated Sn-Beta.

The ^{119}Sn NMR spectra of ^{119}Sn-Beta after calcination and exposure to ambient conditions, which allows the Sn centers to become hydrated, shows a main resonance centered at −688 ppm (Figure 2a) for octahedrally coordinated framework

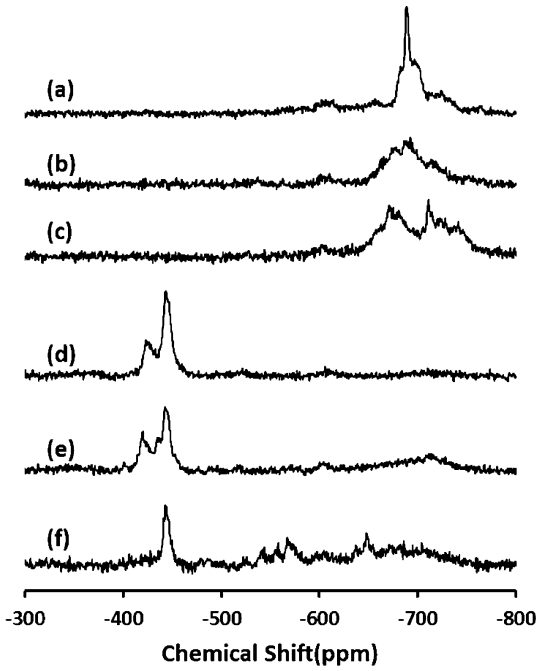

Figure 2. ^{119}Sn MAS solid state NMR spectra of ^{119}Sn-Beta after different treatments: (a) calcination, (b) three Na-exchanges after calcination, (c) NH_3 adsorption after calcination, (d) dehydration after calcination, (e) dehydration after three Na-exchanges, and (f) dehydration after NH_3 adsorption.

Sn.[1,2,25] Upon treatment in vacuum at 393 K to remove the coordinating water, the Sn resonances shift to −423 and −443 ppm (Figure 2d) that are characteristic of tetrahedrally coordinated framework Sn. We have shown previously through ^{1}H−^{119}Sn CPMAS NMR that the open and closed sites correspond to the resonances centered at −423 and −443 ppm, respectively, because only the −423 ppm resonance was detected when cross-polarization occurred from nearby protons.[2]

Three Na-exchanges performed on ^{119}Sn-Beta decrease the intensity of the sharp −688 ppm resonance (Figure 2a) and form a broad shoulder that begins at −650 ppm and merges into the broader features of the ^{119}Sn-Beta NMR spectrum (Figure 2b). ^{119}Sn NMR spectra for samples after dehydration treatments (vacuum at 398 K, 2h) are shown in Figure 2d−f, with magnified spectra spanning the chemical shift range from −400 to −480 ppm shown in Figure S.20 of the Supporting Information. Dehydration of the triply-Na-exchanged ^{119}Sn-Beta shows that the introduction of Na^+ to the sample causes a shift of the open Sn site resonance at −423 ppm (Figure 2d) to −419 ppm (Figure 2e) but does not shift the closed site resonance at −443 ppm (Figure 2d and e). The ^{119}Sn-Beta NMR spectrum of the dehydrated triply-Na-exchanged ^{119}Sn-Beta also contains a small shoulder at −435 ppm that was confirmed not to be a spinning sideband of another resonance (Figure 2e). The ^{1}H−^{119}Sn CPMAS NMR spectrum of dehydrated triply-Na-exchanged ^{119}Sn-Beta shows a resonance at −419 ppm, indicating that these Sn centers have a proton source nearby that cross-polarizes the ^{119}Sn atom (Figure S.21). This observation suggests that Na exchanges only one of the two available protons present in the silanol and stannanol groups in the dehydrated open Sn site (Scheme 1b). The silanol proton is the more likely position for Na exchange (Scheme 1c) in light of the proposed mechanisms for glucose isomerization and epimerization on Sn-Beta that require bonding to glucose through the stannanol group.[17] We experienced difficulties in optimizing ^{1}H−^{119}Sn CPMAS conditions, partly due to poor rf pulse coverage over 300 ppm during contact period at high spinning speeds (14 kHz in this case), that led us to acquire ^{1}H−^{119}Sn CPMAS spectra (e.g., Figure S.21b) by averaging over 30 000 transients. The resonances detected in the tetrahedral range of the dehydrated Na-exchanged ^{119}Sn-Beta do not allow us to characterize the origin of the small −435 ppm shoulder (Figure 2e).

Adsorption of ammonia onto ^{119}Sn-Beta gives rise to two groups of broad resonances centered at −669 and −708 ppm (Figure 2c). Dehydration of this sample (evacuation at 393 K, 2 h) gives rise to a resonance for the closed tetrahedral site (−443 ppm, Figure 2f) but not for the open tetrahedral site found in ^{119}Sn-Beta (−423 ppm, Figure 2d). New resonances are detected in the dehydrated spectrum of Na-^{119}Sn-Beta in the −500 to −600 ppm range, suggesting the presence of a different Sn coordination environment, which may originate from the open site of Sn-Beta depicted in Scheme 1d. The ^{1}H−^{119}Sn CPMAS NMR spectrum of the ^{119}Sn-Beta dehydrated after ammonia adsorption confirms that there is no proton source in the neighborhood of the closed site (−443 ppm), or of any tetrahedrally coordinated Sn sites, after these treatments (Figure S.22).

These ^{119}Sn NMR results are consistent with the interpretations of the IR spectra of Sn-Beta-NH_3 after CD_3CN adsorption, and lead us to propose the Sn structures and coordinations in Scheme 2. Our findings suggest that the open Sn site is a stronger Lewis acid site than the closed Sn site (Scheme 2a), and that it retains adsorbed NH_3 (Scheme 2b) after vacuum treatment at 373 or 393 K (Scheme 2c). Open Sn sites that coordinate one NH_3 ligand would appear as penta-coordinated Sn sites in ^{119}Sn NMR spectra, which we *speculate* could give rise to the resonances detected in −500 to −600 ppm range (Figure 2f). Penta-coordinated open Sn sites with one NH_3 ligand would also bind CD_3CN more weakly than open Sn sites without coordinated NH_3, and may give rise to the 2270 cm^{-1} CD_3CN band observed in IR spectra (Figure 1c). These NMR data also suggest that NH_3 bound to the closed Sn sites desorbs upon dehydration (Scheme 2c), such that the behavior of the closed Sn sites in Sn-Beta-NH_3 is similar to their behavior in Sn-Beta samples that have not been treated with NH_3.

dx.doi.org/10.1021/cs500466j | *ACS Catal.* 2014, 4, 2288−2297

3.3. Mannose Formation with Na Containing Sn-Beta.

Glucose conversion and fructose and mannose yields after reaction with different Sn-Beta samples in water and methanol (1:100 Sn/glucose ratio, 353 K) for 30 min are given in Table 2 (data at 10 and 20 min given in Table S.1). Fructose is the predominant product formed when Sn-Beta reacts with 1% aqueous glucose solutions (Table 2), with carbon balances (84%) that were similar to those we have reported previously.[3] Incomplete closure of carbon balances likely reflects the formation of side products, such as carboxylic acids via retro-aldol reactions of sugars.[26] We have previously shown, using solid state ^{13}C MAS NMR, that these side products are present in zeolites after adsorption of sugars on Sn-Beta in water at ambient temperature,[1] demonstrating that the formation of side products occurs at early reaction times and that these products remain adsorbed on the zeolite after reaction. In order avoid complications in data analysis associated with sugar degradation side reactions that become more prevalent at higher conversions, we focus here on low glucose conversions (<30%) and the initial fructose and mannose products formed.

Table 2. Glucose Conversion (X) and Fructose and Mannose Yields (Y) in H_2O and CH_3OH Solvents[a]

catalyst	solvent	$X_{Gluc.}$ (%)	$Y_{Fruc.}$ (%)	$Y_{Mann.}$ (%)
Sn-Beta	H_2O	6.4	5.0	0.4
	CH_3OH	23.2	10.3	3.9
Sn-Beta-1Ex	H_2O	6.0	2.1	1.8
	CH_3OH	12.6	3.2	5.0
Sn-Beta-2Ex	H_2O	6.1	1.8	2.5
	CH_3OH	12.2	2.1	6.7
Sn-Beta-3Ex	H_2O	6.8	2.3	3.3
	CH_3OH	12.4	0.0	7.9
Sn-Beta-AW	H_2O	5.4	3.9	0.0
	CH_3OH	16.9	6.1	2.8
Na-Sn-Beta-100	H_2O	6.8	5.1	1.1
	CH_3OH	19.4	8.4	3.3
Na-Sn-Beta-60	H_2O	7.3	4.0	2.7
	CH_3OH	17.2	8.0	3.0
Na-Sn-Beta-30	H_2O	5.8	1.1	3.5
	CH_3OH	6.8	0.0	4.6
Sn-Beta-NH_3	H_2O	3.8	1.9	2.4
	CH_3OH	3.0	0.0	1.9
Sn-Beta-NH_3-Cal	H_2O	5.0	3.2	0.0
	CH_3OH	17.6	7.2	2.6

[a]Reaction conditions: 1% (w/w) glucose solutions, 1:100 metal/glucose ratio, 353 K, 30 min.

In water, Na-exchanged Sn-Beta samples led to similar glucose conversions (6.0–6.8%, Table 2) as Sn-Beta (6.4%, Table 2) at equivalent reaction conditions. However, the mannose yield increased systematically from 0.4% to 3.3%, and the fructose yields decreased from 5.0% to ~2% with increasing Na content (Table 2). Similar results were observed with increasing Na content for Na-Sn-Beta samples synthesized directly (Table 2), suggesting that these selectivity differences do not depend on the method used to introduce Na^+ cations into Sn-Beta.

Equivalent reaction conditions in methanol led to higher glucose conversions on Sn-Beta (23.2%) and Na-containing Sn-Beta samples (12.2–12.6%) than in water (Tables 2 and S.1). As in the case of water, mannose yields increased systematically from 3.9% to 7.9%, and fructose yields decreased systematically from 10.3% to 0.0% with increasing Na/Sn ratio (Table 2). Similarly, increasing the sodium content in the synthesis gel of Sn-Beta led to samples that produced higher mannose yields and lower fructose yields (0.0% fructose for Na-Sn-Beta-30, Table 2). The large black particles of the amorphous phase impurity formed from synthesis gels with Si/Na ratios less than 30 were isolated from the crystalline solids and did not react with glucose in water, but were able to catalyze glucose–fructose isomerization in methanol.

Na-containing Sn-Beta catalysts showed a higher selectivity toward mannose for reactions in methanol than in water, and fructose/mannose ratios significantly increased with increasing reaction time for reactions in water (Tables 2 and S.1). These results suggest that sodium decationation could be occurring in aqueous media at a rate that would cause the selectivity to change over the time frame of the experiment. Thus, we investigated the effects of adding sodium salt to the aqueous reaction solution in order to maintain the sodium content in the solid more effectively during reaction (Tables 3 and S.2).

Table 3. Glucose Conversion (X) and Fructose and Mannose Yields (Y) with 0.2 g NaCl/g H_2O[a]

catalyst	solvent	$X_{Gluc.}$ (%)	$Y_{Fruc.}$ (%)	$Y_{Mann.}$ (%)
Sn-Beta[b]	H_2O-NaCl	9.8	4.5	4.1
Sn-Beta-1Ex	H_2O-NaCl	10.9	2.6	5.2
Sn-Beta-2Ex	H_2O-NaCl	10.7	2.5	6.0
Sn-Beta-3Ex	H_2O-NaCl	11.5	0.0	7.5

[a]Reaction conditions: 1% (w/w) glucose solutions, 1:100 metal/glucose ratio, 353 K, 30 min. [b]After reaction the catalyst had a Si/Sn and a Na/Sn ratio of 115 ± 30 and 2.65 ± 1.25, respectively, determined by Energy Dispersive X-ray Spectroscopy (EDS).

When glucose was reacted with Sn-Beta in aqueous NaCl solutions, mannose and fructose were produced in nearly equal yields (4.1% and 4.5%, respectively; Tables 3 and S.2), and the solid had a Na/Sn ratio of 2.65 after reaction (Tables 3 and S.2) indicating that Na^+ was exchanging into the solid during reaction. Sn-Beta pre-exchanged with Na^+ (Sn-Beta-3Ex) maintained constant mannose selectivity during the course of the reaction when NaCl was added to the aqueous reaction solutions. No fructose or mannose formation was observed without Sn-Beta in aqueous NaCl solution, showing that NaCl does not catalyze isomerization reactions of glucose. These results indicate that the presence of a sodium cation, whether added synthetically or exchanged onto the material prior to or during the reaction, shifts the reaction selectivity of Sn-Beta from isomerization to fructose to epimerization to mannose. In water solvent, the Na^+ ion in the active site is replaced by a proton, causing a reversal towards the active site structure that predominantly forms fructose, while in methanol the Na^+ ion is retained in the active site for longer times, resulting in formation of mannose as the major product. The addition of excess sodium salt to aqueous reaction mixtures increases the extent to which Na^+ exchanges onto Sn-Beta, in turn maintaining the selectivity toward mannose during the course of reaction.

The Sn-Beta sample that was dosed with NH_3 showed lower glucose conversions in both water and methanol solvents (3.0–3.8%, Table 2) than Sn-Beta and the Na-containing Sn-Beta samples. Higher glucose conversions were observed with Sn-Beta-NH_3 in water and resulted in a dark yellow postreaction solution, which may indicate the presence of humins formed

dx.doi.org/10.1021/cs500466j | ACS Catal. 2014, 4, 2288–2297

from NH_4OH that may have formed *in situ* from the desorption of NH_3. Calcination of the ammonia-dosed sample led to a nearly full recovery of the reactivity in methanol and water (17.6% and 5.0% glucose conversion, respectively, Table 2). The suppression of isomerization reactivity on Sn-Beta-NH_3 (Table 2) occurs together with the disappearance of the open site CD_3CN IR band at 2315 cm^{-1} (Figure 1c) and with the disappearance of the open site ^{119}Sn NMR resonance at −423 ppm (Figure 2f) in the dehydrated NH_3-dosed Sn-Beta. These data corroborate our proposal that the open site is the active site for the isomerization of glucose to fructose in the absence of sodium and is the active site for the epimerization of glucose to form mannose in the presence of sodium.

3.4. Sodium Removal from Sn-Beta. The Sn-Beta-3Ex sample was acid washed to remove Na^+ from the sample (Sn-Beta-AW) and probe whether the effects of sodium on the reactivity of Sn-Beta were reversible. Sn-Beta-AW had much less sodium (Na/Sn = 0.27) than Sn-Beta-3Ex (Na/Sn = 4.85). The glucose conversion and the fructose and mannose yields observed with Sn-Beta-AW were very similar to that of the parent Sn-Beta (Table 2). The decrease in mannose yield and concurrent increase in fructose yield after the acid treatment demonstrates that the effects of sodium addition are reversible and are not a result of a permanent poisoning of the site active for glucose−fructose isomerization.

The effect of the reaction solvent on the recyclability of the catalyst was probed by reacting Sn-Beta-3Ex with glucose in water and methanol under the previously stated reaction conditions (353 K for 30 min in a 1% (w/w) glucose solution) and washing once with the solvent used in the reaction. This cycle was repeated twice, and the reaction results after each cycle are shown in Table 4. The Na/Sn ratio of the material

Table 4. Glucose Conversion (X) and Fructose and Mannose Yields (Y) with Sn-Beta-3Ex in CH_3OH and H_2O[a]

Cycle	Si/Sn[b]	Na/Sn[b]	Solvent	$X_{Gluc.}$(%)	$Y_{Fruc.}$(%)	$Y_{Mann.}$(%)
1	115	4.38	H_2O	8.5	1.7	4.5
2	136	0.93	H_2O	8.6	4.6	3.9
3	123	0.26	H_2O	9.0	6.4	1.2
1	115	4.38	CH_3OH	9.4	0.0	6.5
2	132	1.26	CH_3OH	10.2	1.5	6.0
3	119	0.82	CH_3OH	13.7	3.7	6.2

[a]After the first cycle the catalysts were washed with the solvent used in the reaction and reused under the same reaction and solvent conditions as the previous cycle. Reaction conditions: 1% (w/w) glucose solutions, 1:100 metal/glucose ratio, 353 K, 30 min. [b]Determined by Energy Dispersive X-ray Spectroscopy (EDS). Uncertainty in Si/Sn is ±30. Uncertainty in Na/Sn is ±1.25.

decreased in each cycle, with a greater extent of sodium loss in the case of aqueous media. A decrease in sodium content in the zeolite after each cycle also led to a decrease in the mannose yield and corresponding increase in the fructose yield (Table 4), consistent with the proposal that open Sn sites with Na-exchanged silanol groups are active sites for the epimerization reaction.

3.5. Glucose Isomerization and Epimerization Mechanisms. One percent (w/w) glucose labeled with ^{13}C at the C1 position (^{13}C-C1-glucose) was reacted at 353 K for 30 min with Sn-Beta in water, aqueous NaCl solutions (0.2 g NaCl/g H_2O), and methanol as solvents to determine the mechanisms of glucose isomerization to fructose and epimerization to mannose. All ^{13}C NMR spectra in Figure 3 show the presence of ^{13}C in the C1 position (resonances at δ = 95.8 and 92.0

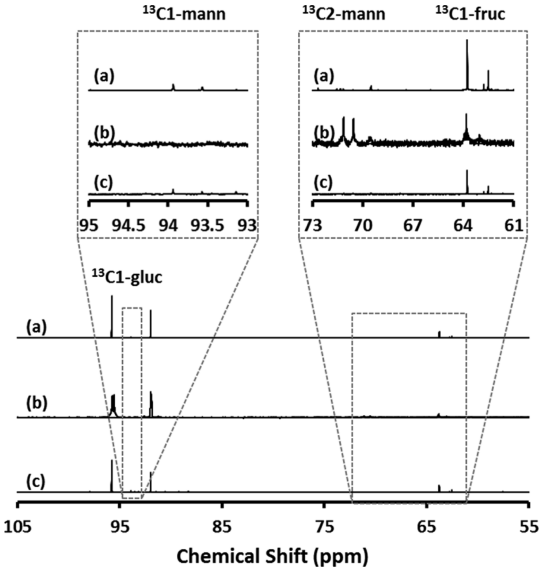

Figure 3. ^{13}C NMR spectra for reactant and products with Sn-Beta in a 1% (w/w) ^{13}C-C1-glucose solution at 353 K for 30 min with the following solvent mixtures (a) H_2O, (b) NaCl-H_2O, and (c) CH_3OH. The abbreviations "gluc," "fruc," and "mann" stand for glucose, fructose, and mannose, respectively.

ppm) of the α and β pyranose forms of the starting labeled glucose, respectively. The fructose formed from reactions with Sn-Beta in all three solvents showed ^{13}C in the C1 position (resonances at δ = 63.8 and 62.6 ppm) for β-pyranose and β-furanose forms of fructose, as expected from isomerization mediated by 1,2 intramolecular hydride shift.[1] The ^{13}C label was only observed in the C1 position (resonances at δ = 93.9 and 93.5 ppm) of α and β pyranose forms of mannose with water and methanol solvents in Sn-Beta, indicating that mannose was not formed by a 1,2 intramolecular carbon shift, but likely via 1,2 intramolecular hydride shift of fructose products into mannose. In contrast, the ^{13}C label appeared in the C2 position (resonances at δ = 70.5 and 71.1 ppm) of the α and β pyranose forms of mannose with Sn-Beta in aqueous NaCl solutions, indicating that mannose was formed by the 1,2 intramolecular carbon shift mechanism of the Bilik reaction.[9]

The isotopic labeling experiments performed with Sn-Beta were also conducted with Sn-Beta-3Ex in water, aqueous NaCl solutions (0.2 g NaCl/g H_2O), and methanol as solvents, and the resulting ^{13}C NMR spectra are shown in Figure 4. In water, the fructose products retained the ^{13}C label in the C1 position (resonances at δ = 63.8 and 62.6 ppm), with a lower intensity relative to Sn-Beta, and the mannose product showed the ^{13}C label only in the C2 position (resonances at δ = 70.5 and 71.1 ppm). These results, together with reaction data for earlier reaction times in Table S.2, suggest that Sn-Beta-3Ex initially forms mannose through the 1,2 intramolecular carbon shift in water, but the loss of sodium from the active site results in the formation of fructose without carbon rearrangement. When methanol or concentrated aqueous NaCl solutions were used as solvents, mannose with ^{13}C in the C2 position was observed as the main product. These results confirm that the switch in reaction mechanism from isomerization to epimerization of

dx.doi.org/10.1021/cs500466j | ACS Catal. 2014, 4, 2288−2297

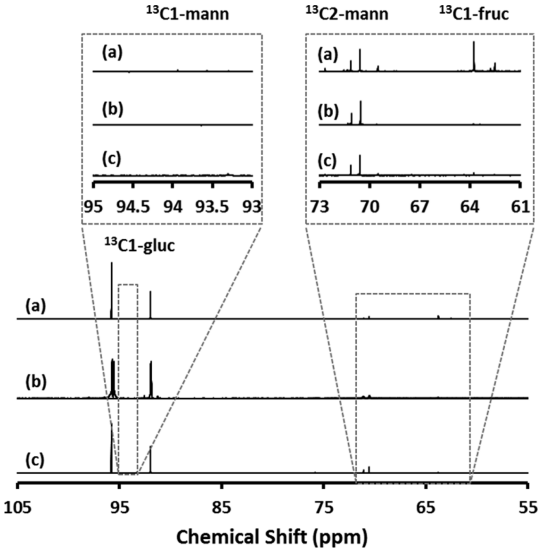

Figure 4. ^{13}C NMR spectra for reactant and products with Sn-Beta-3Ex in a 1% (w/w) ^{13}C-C1-glucose solution at 353 K for 30 min with the following solvent mixtures: (a) H_2O, (b) NaCl-H_2O, and (c) CH_3OH. The abbreviations "gluc," "fruc," and "mann" stand for glucose, fructose, and mannose, respectively.

sodium-exchanged materials is not directly dependent on the solvent but rather on the presence of sodium in the active site.

Glucose epimerization into mannose can proceed via reversible enolization upon abstraction of α-carbonyl protons (LdB–AvE rearrangement), or via an intramolecular carbon shift between C1 and C2 positions.[27] In order to confirm that the Sn-Beta containing Na^+ was not epimerizing glucose to mannose by abstraction of the α-carbonyl proton, glucose with deuterium at the C2 position (glucose-D2) was used as a reactant. The mannose formed with Sn-Beta-3Ex after 30 min at 353 K with 1% (w/w) glucose solution in methanol did not show resonances at δ = 93.9 and 93.5 ppm (Figure 5) that correspond to the C1 positions of the α and β pyranose forms

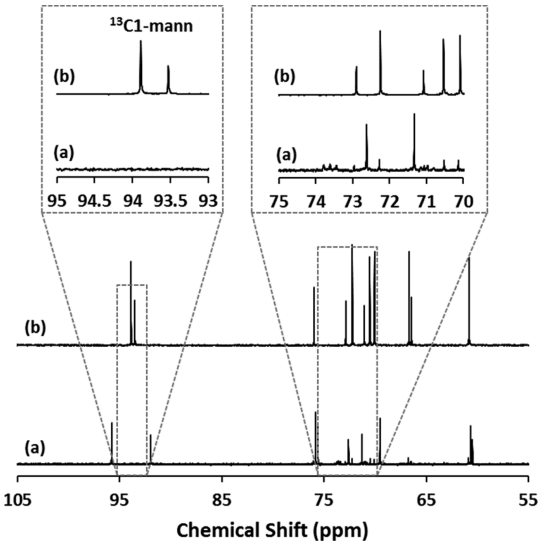

Figure 5. ^{13}C NMR spectra for (a) reactant and products with Sn-Beta-3Ex in a 1% (w/w) ^{13}C-C1-glucose solutions at 353 K for 30 min in CH_3OH and (b) mannose. The abbreviation "mann" stands for mannose.

of mannose, respectively. This NMR evidence indicates that with the sodium cation in the active site of Sn-Beta, the carbon in the C2 position of glucose moves along with its deuterium to the C1 position by the 1,2 intramolecular carbon shift to form mannose, as we have observed previously.[2] It is clear that the presence of alkali metal cations in Sn-Beta can determine whether epimerization can occur. In our initial report on glucose epimerization into mannose via 1,2 intramolecular carbon shift with Sn-Beta in methanol,[2] we did not purposefully add alkali metal cations to the synthesis gel for crystallizing Sn-Beta. We have analyzed the samples used in that study and found them to contain potassium. Although the exact origin of the potassium remains unknown to us at this time, its presence in those samples is likely the reason why we observed epimerization of glucose in methanol solvent.

4. CONCLUSION

Partially hydrolyzed Sn sites in zeolite beta (denoted as open Sn sites) with proximal silanol groups are shown to be the active sites for the isomerization of glucose into fructose via a Lewis-acid mediated 1,2 hydride shift mechanism. The exchange of Na^+ onto the adjacent silanol group of the open Sn sites results in sites that are active for the epimerization of glucose into mannose via a 1,2 intramolecular carbon shift. Na^+ cations can be exchanged onto silanol groups in active Sn sites of Sn-Beta either by postsynthetic ion exchange or by addition of low amounts of $NaNO_3$ during synthesis. Acid washing of Na-exchanged Sn-Beta resulted in nearly full recovery of the initial reactivity of the parent alkali-free Sn-Beta, thereby showing that any alterations to the active sites by Na^+ are reversible. Na^+ cations remain exchanged onto Sn-Beta in methanol solvent, but decationation occurs gradually with increasing reaction time in aqueous solvent. The addition of NaCl to aqueous reaction solutions appeared to preserve Na^+ cations exchanged onto silanol groups, as it led to an enhancement in the selectivity toward epimerization of glucose into mannose. These findings, in combination with recyclability studies performed in water and methanol, indicate that Na^+ cations are labile under reaction conditions and that the nature of the solvent influences their lability.

■ ASSOCIATED CONTENT

Supporting Information

Catalyst characterization (X-ray diffractograms, SEM images, and IR and solid state NMR spectra) and additional reaction data are provided. This material is available free of charge via the Internet at http://pubs.acs.org/.

■ AUTHOR INFORMATION

Corresponding Author

*E-mail: mdavis@cheme.caltech.edu.

Present Address

[†]School of Chemical Engineering, Purdue University, 480 Stadium Mall Drive, West Lafayette, IN 47907

Author Contributions

[‡]R.B.D. and M.O. contributed equally to this work.

Notes

The authors declare no competing financial interest.

■ ACKNOWLEDGMENTS

This work was financially supported as part of the Catalysis Center for Energy Innovation, an Energy Frontier Research

Center funded by the U.S. Department of Energy, Office of Science, Office of Basic Energy Sciences under Award Number DE-SC0001004. M.O. wishes to acknowledge funding from the National Science Foundation Graduate Research Fellowship Program under Grant No. DGE-1144469. Any opinions, findings, and conclusions or recommendations expressed in this material are those of the author(s) and do not necessarily reflect the views of the National Science Foundation.

REFERENCES

(1) Bermejo-Deval, R.; Assary, R. S.; Nikolla, E.; Moliner, M.; Román-Leshkov, Y.; Hwang, S.-J.; Palsdottir, A.; Silverman, D.; Lobo, R. F.; Curtiss, L. A.; Davis, M. E. *Proc. Natl. Acad. Sci. U. S. A.* **2012**, *109*, 9727−9732.
(2) Bermejo-Deval, R.; Gounder, R.; Davis, M. E. *ACS Catal.* **2012**, *2*, 2705−2713.
(3) Moliner, M.; Román-Leshkov, Y.; Davis, M. E. *Proc. Natl. Acad. Sci. U. S. A.* **2010**, *107*, 6164−6168.
(4) Nikolla, E.; Román-Leshkov, Y.; Moliner, M.; Davis, M. E. *ACS Catal.* **2011**, 408−410.
(5) Collyer, C. A.; Henrick, K.; Blow, D. M. *J. Mol. Biol.* **1990**, *212*, 211−235.
(6) Bhosale, S. H.; Rao, M. B.; Deshpande, V. V. *Microbiol. Rev.* **1996**, *60*, 280−300.
(7) Kovalevsky, A. Y.; Hanson, L.; Fisher, S. Z.; Mustyakimov, M.; Mason, S. A.; Forsyth, V. T.; Blakeley, M. P.; Keen, D. A.; Wagner, T.; Carrell, H. L.; Katz, A. K.; Glusker, J. P.; Langan, P. *Structure* **2010**, *18*, 688−699.
(8) Roy, S.; Bakhmutsky, K.; Mahmoud, E.; Lobo, R. F.; Gorte, R. J. *ACS Catal.* **2013**, *3*, 573−580.
(9) Hayes, M. L.; Pennings, N. J.; Serianni, A. S.; Barker, R. *J. Am. Chem. Soc.* **1982**, *104*, 6764−6769.
(10) Petrus, L. *Chem. Zvesti (1947-1984)* **1975**, *29*, 690−693.
(11) Bílik, V.; Petrus, L.; Zemek, J. *Chem. Zvesti (1947-1984)* **1978**, *32*, 242−251.
(12) Tanase, T.; Shimizu, F.; Kuse, M.; Yano, S.; Yoshikawa, S.; Hidai, M. *J. Chem. Soc., Chem. Commun.* **1987**, *2*, 659.
(13) Tanase, T.; Shimizu, F.; Yano, S.; Yoshikawa, S. *J. Chem. Soc., Chem. Commun.* **1986**, 1001−1003.
(14) Tanase, T.; Shimizu, F.; Kuse, M.; Yano, S.; Hidai, M.; Yoshikawa, S. *Inorg. Chem.* **1988**, *27*, 4085−4094.
(15) Boronat, M.; Concepcion, P.; Corma, A.; Renz, M.; Valencia, S. *J. Catal.* **2005**, *234*, 111−118.
(16) Khouw, C.; Davis, M. E. *J. Catal.* **1995**, *151*, 77−86.
(17) Rai, N.; Caratzoulas, S.; Vlachos, D. G. *ACS Catal.* **2013**, *3*, 2294−2298.
(18) Gounder, R.; Davis, M. E. *J. Catal.* **2013**, *308*, 176−188.
(19) Faggin, M. F.; Hines, M. A. *Rev. Sci. Instrum.* **2004**, 75.
(20) Bellussi, G.; Fattore, V. In *Zeolite Chemistry and Catalysis Proceedings of an International Symposium*; Jacobs, P. A., Jaeger, N. I., Kubelková, L., Wichterlova, B., Eds.; Elsevier: Amsterdam, 1991; Vol. *69*, pp 79−92.
(21) Miller, F. A.; Wilkins, C. H. *Anal. Chem.* **1952**, *24*, 1253−1294.
(22) Pelmenschikov, A. G.; van Santen, R. A.; Jänchen, J.; Meijer, E. *J. Phys. Chem.* **1993**, *97*, 11071−11074.
(23) Wichterlová, B.; Tvarůžková, Z.; Sobalík, Z.; Sarv, P. *Microporous Mesoporous Mater.* **1998**, *24*, 223−233.
(24) Boronat, M.; Concepción, P.; Corma, A.; Navarro, M. T.; Renz, M.; Valencia, S. *Phys. Chem. Chem. Phys.* **2009**, *11*, 2876−2884.
(25) Corma, A.; Nemeth, L. T.; Renz, M.; Valencia, S. *Nature* **2001**, *412*, 423−425.
(26) Holm, M. S.; Saravanamurugan, S.; Taarning, E. *Science* **2010**, *328*, 602−605.
(27) Osanai, S. *Top. Curr. Chem.* **2001**, *215*, 43−76.